XVIII IMEKO WORLD CONGRESS
Metrology for a Sustainable Development
September, 17 – 22, 2006, Rio de Janeiro, Brazil

SI REALIZATION OF SMALL FORCES USING AN ELECTROSTATIC FORCE BALANCE

Jon R. Pratt [1], *John A. Kramar* [2]

[1] National Institute of Standards and Technology, Gaithersburg, MD, USA, jon.pratt@nist.gov
[2] National Institute of Standards and Technology, Gaithersburg, MD, USA, john.kramar@nist.gov

Abstract: We describe the realization of micronewton forces in a fashion traceable to the International System of Units (SI) using the National Institute of Standards and Technology (NIST) electrostatic force balance. A comparison between deadweight and electrostatic force is presented at a force level of approximately 200 μN. Our results demonstrate agreement between these two independent measurements at a level consistent with the uncertainties in 20 mg mass artifacts. We provide a brief description of our balance and its measurement principles, and then outline the procedures and the data analysis used to derive our results. As part of the paper, we also present a table that summarizes the uncertainties associated with realizing a 200 μN force via an electrode suspended in a measured electrostatic field. We compare this with the uncertainties associated with realizing the same force via a mass artifact in a measured gravitational field.

Keywords: electrostatic force balance, atomic force microscope, instrumented indentation, force calibration, standard references and practices, small force measurement.

1. INTRODUCTION

The accurate determination of forces at the level of 200 μN and below is of great interest in the general areas of nanomechanics, single molecule biophysics, and molecular electronics. Force-displacement curves measured using instrumented indentation machines, surface forces apparatuses, atomic force microscopes, and optical tweezers have been used to determine the elastic properties of materials at surfaces [1], interaction potentials [2], and to characterize the change in molecular conformation associated with DNA melting transitions [3]. Most of these measurements are relative in nature, but absolute accuracy is desired, even among the atomic force microscope (AFM) community, where the quest for accurate measurement of cantilever spring constants forms a substantial literature [4].

The NIST small force metrology laboratory was established to provide a traceability link to the SI for force measurement and testing instruments in the range below 10 mN [5]. Of particular interest has been the establishment of instrumentation and procedures to allow the realization of SI-traceable forces below 10 μN. This topic was introduced as part of a previous IMEKO paper [6] and here we present an update on our progress.

2. OBJECTIVE

We have shown previously that it is possible to use the determination of the volt, farad, and meter as realized within the SI in conjunction with an electrostatic force balance to link small mechanical forces to the SI [7]. We have also calibrated AFM force sensors by pressing them against this electrostatic force balance [8]. Recently, the direct application of electrostatic forces in a micro-electro-mechanical system (MEMS) device has been proposed as a means for producing an AFM spring constant artifact potentially traceable to the SI [9]. Our objective here is to communicate the accuracy of recent NIST electrostatic force balance experiments and to suggest that at the few milligram level, mass could in principle be derived from the electrical units with no loss in uncertainty.

3. METHODOLOGY

At NIST, we realize a primary standard of small force from electrostatics, and have constructed a series of increasingly refined systems to realize force using a coaxial cylindrical capacitor arrangement [5,7]. The present version of this primary standard, referred to as the NIST Electrostatic Force Balance, or simply the EFB, is shown schematically in the drawing of Fig. 1.

As shown in the drawing, the balance has been assembled on a custom optical table in a specially designed free standing vacuum chamber approximately 1 m in diameter. The optical table on which the EFB is mounted sits on three legs that protrude from the chamber floor through flexible bellows that terminate in blank flanges. These table legs are supported from below the chamber by a large granite block, as indicated schematically in Fig. 1. Thus, the only contact between the vacuum chamber and the experiment is through the relatively compliant bellows. The experiment can operate in air, but vacuum operation eliminates convective air currents that tend to perturb the large and compliant balance suspension. Also, operation in vacuum eliminates the need to correct for the index of refraction in the interferometer and changes in the dielectric constant of the gap in the capacitor.

Functionally, the EFB consists of an electrostatic force generator that acts along a vertical axis (z-direction) aligned to the local gravity to within a few milliradians. Forces are generated when voltages are applied to the pair of nested, coaxial cylinders (Fig. 1, items 3 and 4). The outer high-

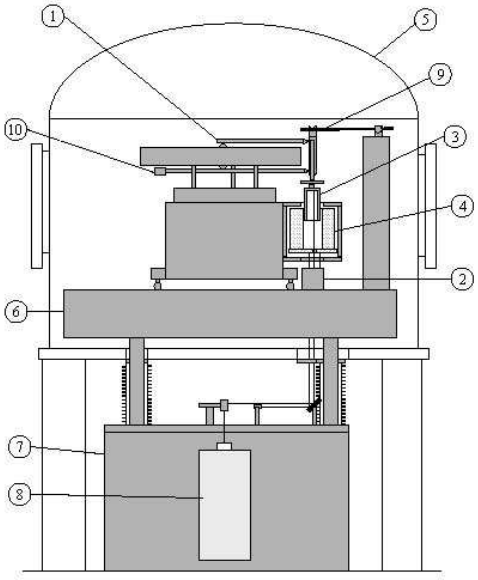

Fig. 1. Schematic of balance components: 1) Parallelogram balance 2) Differential plane mirror interferometer 3) Main inner electrode (cross-section) 4) Main outer electrode (cross-section) 5) Vacuum chamber 6) Optical table 7) Granite foundation block 8) Heterodyne laser light source 9) Mass lift 10) Counterweight

voltage cylinder is fixed while the inner electrically-grounded cylinder is free to translate along the *z* axis, varying the degree of overlap. The capacitance of this geometry is in principle a linear function of the overlap of the two cylinders. For a perfectly coaxial arrangement, the in-plane capacitance gradient possesses radial symmetry so that the resulting electrical force is directed solely along the z-axis. To define this axis of symmetry, the inner cylinder is suspended from a counterbalanced parallelogram linkage (Fig. 1, item 1) that employs a series of crossed-flexure pivots. This mechanism produces a well-constrained motion axis, easily aligned to gravity, that is largely insensitive to off-axis forces, while the on-axis stiffness can be varied to as small as 0.001 N/m through the use of a novel tensioning spring [6].

The NIST electrostatic force balance generates electrical forces, F_e, in response to loads along the balance axis that may be calculated from

$$F_e = \frac{1}{2}\frac{dC}{dz}(U + U_s)^2 \qquad (1)$$

where dC/dz is the capacitance gradient, U is the voltage applied to the outer electrode, and U_s is the potential difference between the electrodes resulting from surface field effects. To determine U_s, the polarity of the voltage on the outer electrode is reversed with no change in the force load. U_s is one half the difference in the applied voltages. A typical U_s we measure is 0.15 V, but it ranges from 0.1 V to 0.18 V in our experiment.

The balance has two modes of operation, namely a gradient calibration mode and a weighing or force comparison mode. Gradient calibration is accomplished by moving the balance suspension through a small range of motion (typically < ± 0.2 mm) about the null position. A second electrode pair on the counterweight side of the balance is used to drive the balance arm, moving the main inner electrode with respect to the fixed main outer electrode. The capacitance and displacement between the fixed and moving electrodes are recorded, so that the general function $C(z)$ is mapped at discrete locations along the balance motion axis. The function $C(z)$ is plotted, and then fit with a straight line from which the gradient, or local slope is determined.

Weighings and force comparisons are accomplished by controlling the voltage on the main electrodes to maintain the null position of the balance. We use a proportional-integral-derivative (PID) servo controller implemented on a dedicated processor in a separate chassis, with high-level operator control through an ordinary PC. For typical balance operation, a mechanical imbalance is imposed on the counterweight side which is countered by an electrostatic force applied by the controller to maintain null as measured by the interferometer. Positive loads can then be measured on the weighing side of the balance, provided they do not exceed the mechanical imbalance. Typically, loads are applied and removed and a force is calculated from the change in controlled voltage necessary to maintain null.

4. MEASUREMENT

An exhaustive comparison between the gravitational force acting on a 20 mg test mass and the balancing electrostatic force generated by the EFB has been ongoing for a few months. A typical weighing sequence intersperses sets of capacitance gradient (dC/dz) determinations with sets of weighings, each set taking a little over an hour. The dC/dz value used for each weighing is the mean of the neighboring dC/dz measurements, in an effort to account for any linear trend.

Figure 2 is a representative dC/dz set, having 13 bidirectional cycles of three-point sweeps. Each point within the sweep is averaged for about 30 s. The capacitance is measured by a sensitive bridge circuit, and the displacement by an interferometer system. To test the validity of using three points to estimate dC/dz, a set of capacitance measurements with eleven point sweeps was

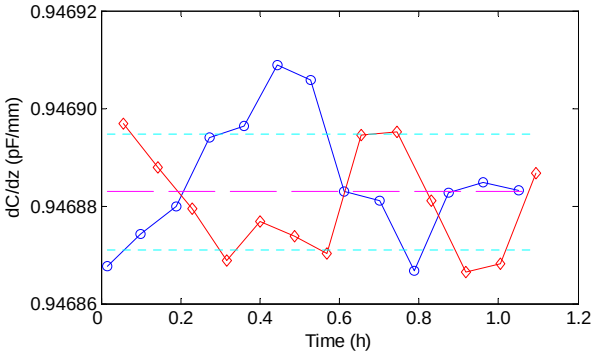

Fig. 2. A *dC/dz* weighing set. Each point is a slope calculated from a set of three points at 0 mm and ± 0.2 mm. The circle data points are slope calculated from positive transversal, the diamond from negative traversal. The symmetric deviation of the two curves with respect to the mean is in part due to drift in the mean capacitance and is not indicative of a change in the physical quantity *dC/dz*. (mean = 0.946907 pF/mm, σ = 3.0 x 10^{-5} pF/mm, σ/√N = 5.0 x 10^{-6} pF/mm)

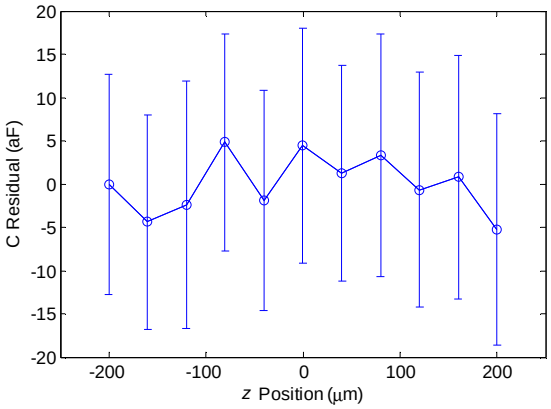

Fig. 3. Capacitance residual after subtraction of a linear fit. The points are averages from 40 bidirectional, eleven point, 400 μm *z* sweeps. The fit *dC/dz* was -0.946756 pF/mm.

measured. The residuals from a linear fit (Fig. 3) are within 1.5×10^{-5} of the total sweep amplitude of 0.4 pF. A mean *dC/dz* value is calculated from each of the one hour sets (*e.g.*, Fig. 2). Figure 4a is a trend line of the *dC/dz* set means over a period of several days. The drift in *dC/dz* is somewhat correlated to rate of change of the temperature (Fig. 4b). As the temperature varies, the total capacitance also changes (Fig. 4c). Although the temperature of the room is controlled typically within ± 0.02 °C, the temperature of the balance components inside the vacuum system vary by as much as 1 °C, especially as the system temperature stabilizes over a period of a day after pump down, or as the power to the *in vacuo* actuators is cycled. The dependence of the capacitance on the temperature is well explained by the thermal expansion of the position of the overlapping edges of the electrodes relative to the measured mirror locations. The dependence of *dC/dz* on the temperature is likely due to the effect it has on the centering of the capacitance electrode cylinders. Since the support structure for the outer cylinder and for the inner cylinder are both aluminum, the equilibrium expansions are expected to be the same, but the outer cylinder support structure is much more thermally massive, and thus will respond more slowly to the temperature changes.

Weighing data sets are commonly 33 mass on-off cycles (Fig. 5). The voltage for each mass on or off condition is averaged for about 30 s. In order to track the surface potential, U_s, the sign of the applied voltage is switched between alternate mass on-off cycles. Typically, the drift in U_s is small, so a single mean U_s is calculated and used to correct all the measured voltages for a given set. Any misestimate of U_s will at worst add a difference to alternate voltage weighings within the set, but will not affect the mean. The electrostatic force for each mass off or mass on condition is calculated based on the corrected voltage and the current estimate of *dC/dz*. Individual weighings are determined as the difference between a mass-on condition force and the mean of the neighboring mass-off condition forces (and vice versa), again to correct for linear drift.

The entire history of the means of weighing data sets for the past four months for this 20 mg artifact are shown in Fig. 6, where we plot the mean electrostatically measured force for each data set. Some of the shifts in measured force

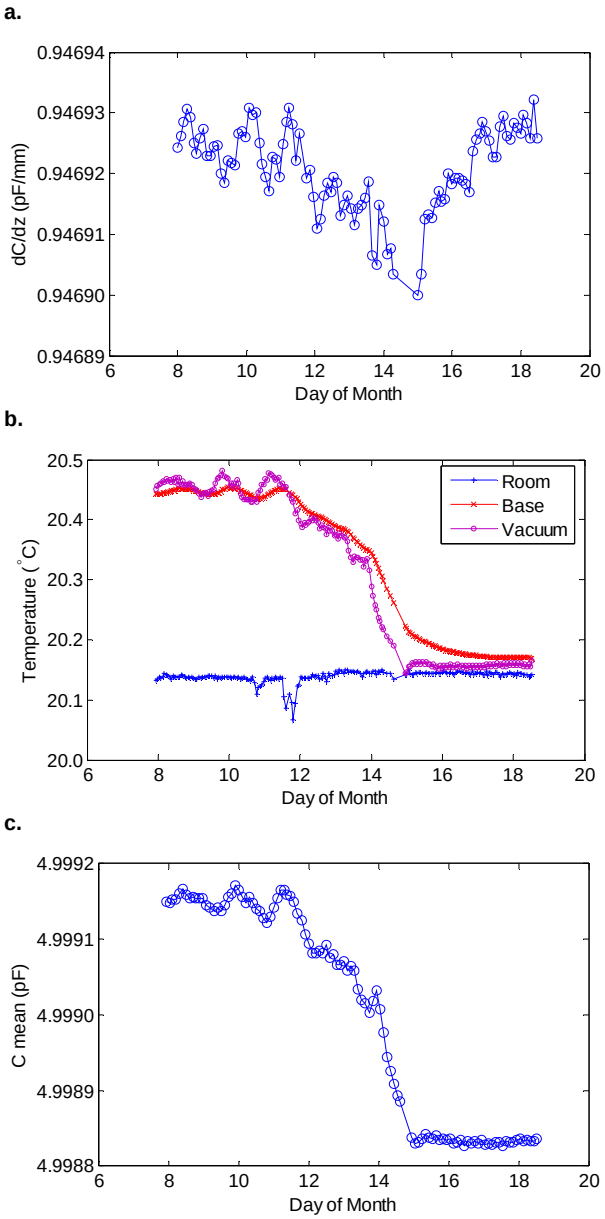

Fig. 4. a) History plot of the mean *dC/dz* for each data set over a period of ten days; b) temperature of vacuum, balance base and room (sensor offsets not calibrated); c) mean capacitance for each data set.

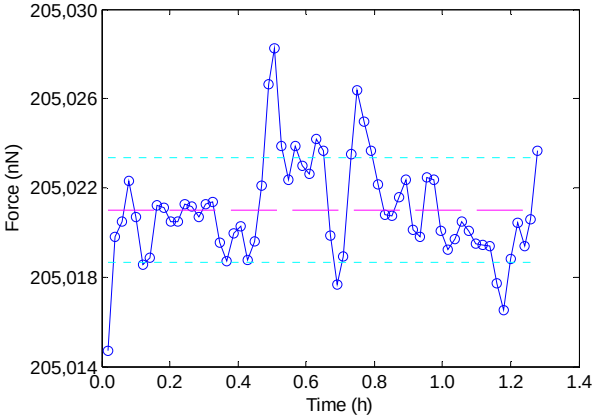

Fig. 5. Typical processed weighing data set for a 20 mg test mass. (mean = 205021.0 nN, σ = 2.4 nN, σ/√N = 0.3 nN)

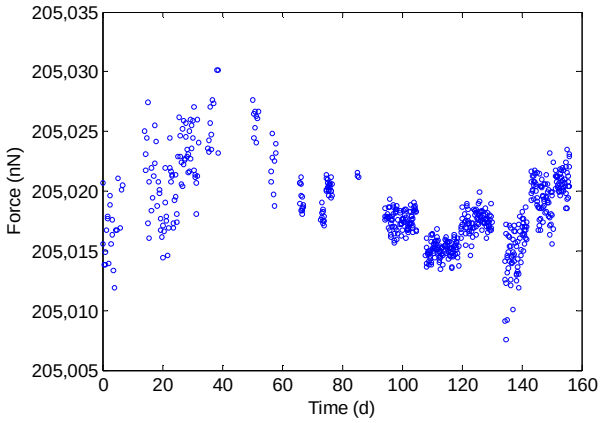

Fig. 6. History of electrostatic force determinations for 20 mg test mass in gravitational field over a 160 d period. (mean = 205018.3 nN, σ = 3.13 nN, σ/√N = 0.12 nN)

seem to be deterministic based on known effects; for others, the origin of the shifts are yet unknown. For example, the broad peak in the force around day 40 correlates to some extent with a failure in the air conditioning system in the control room in which the capacitance bridge and voltmeters were located. The temperature rose by more than 5 °C for a period of a few weeks. (The EFB itself is in a separate temperature controlled room.)

Another point that is apparent from the weighing history is that the measurement noise has generally decreased. This is due to continuing improvements in the balance operations such as better low-noise cabling and the switch-over to a more deterministic, higher bandwidth balance controller; controller servo parameters have also been continually adjusted for optimization.

5. ALIGNMENT AND UNCERTAINTY

Estimates have been made of the sources of measurement uncertainty. A large category of uncertainties is associated with the requisite alignments of the force and measurement axes. Care was taken in the set up to align the inner cylinder translation axis and the interferometer measurement axis with gravity. The starting point is to align a laser beam with gravity by adjusting it for normal reflection off a mirror that has been leveled with a bubble level. To align the balance axis to this reference beam, the beam is reflected through a corner cube mounted on the moving element, and brought back to a position sensitive detector; the lateral motion of the returned beam is monitored as the balance is translated. Effectively, the alignment of the interferometer measurement axis means the alignment of the laser beam and the alignment of the mirror normals of the inner cylinder and outer cylinder mirrors with gravity. All of these angles are adjusted to within 1 mrad, and affect the measurement by a factor of the cosine of the angle, *i.e.*, less than 5×10^{-7}.

A potential source of error in a parallel linkage motion constraint is a lack of accuracy in the relative placement of the flexure pivots or in the length of the arms. In general, this may lead to a parasitic tilt or rotation of the guided motion. While any resulting issues associated with the alignment of the motion axis appear as the cosine of the angle, and in our implementation are quite small, this rotation will also lead to a dependence of the force on the moment arm, known as corner loading error [10], which appears as the sine of the angle times the moment arm. The balance is built with an adjustment to null out this error. The adjustment is made by monitoring with an autocollimator the tilt of a mirror placed on the moving element while the balance is translated. Furthermore, to experimentally verify this adjustment, we compared on-axis weighings with weighings where the mass was offset by 100 mm to magnify the effect. An example of one such experiment is captured in the weighing history (Fig. 6). On days 95 to 105 and 120 to 130 the mass was offset by 100 mm to one side. In between, on days 105 to 120, the mass was centered. Evidently, the magnitude of the corner loading effect at this exaggerated offset is no more than 2 nN or a relative error of 1×10^{-5}. A conservative estimate of the centering of the mass under normal conditions is 3 mm, leading to an uncertainty contribution factor of 3×10^{-7}.

The alignment of the capacitance cylinders with respect to each other is also a consideration. The geometric axes of the cylinders are manufactured to be aligned with the mirror normals to within the comparatively negligible machine tolerance of 10 μrad, thus the alignment of the interferometer mirrors captures the requirement for parallelism of the cylinders to within the previously discussed 1 mrad. The centering of the cylinders is done by adjusting *x* and *y* for minimum capacitance at fixed *z* height, and is conservatively estimated to be within 10 μm. In spite of this adjustment, to the degree that the electrodes are miscentered—and they must be to some extent, at least during temperature excursions—there will be a small lateral component to the electrostatic force. This will apply an unknown moment that must be counteracted by the off-axis stiffness and will have an effect that could couple into the force measurement through cross terms, similar to the corner loading error. Any such effect is expected to be small and is not included in the current uncertainty analysis.

Balance hysteresis is another concern. The electrostatic force required to null the balance is affected by the position history of the balance mechanism. As the mass is loaded on and off, the finite stiffness of the controller allows a transient deviation from the null control point. This

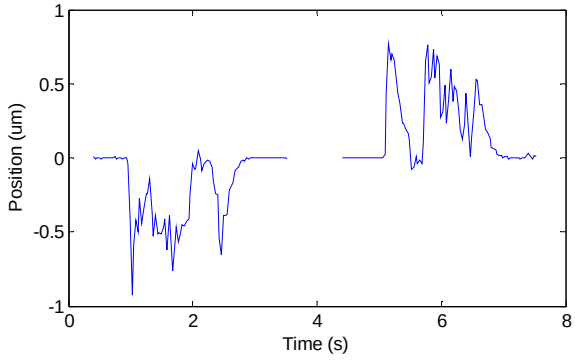

Fig. 7. Null position disturbances caused by typical mass-on and mass-off transitions.

Table 1. Balance Hysteresis force, F_h (nN), for various symmetric excursion amplitudes and times.

time (s)	excursion amplitude (μm)						
	0.3	1	3	10	30	100	200
2		1.5	1.1	3.0	54		
3	0.9	1.5	1.7	4.1	50	69	126
10	1.2	1.6	2.0	5.6	58	83	155
30	1.7	2.8	3.9	9.6	68	115	216
100		3.9	7.1	17.0	91		

disturbance is currently limited to a peak of less than 1 μm with a width of a few seconds (Fig. 7), though it was typically 3 μm for some of the earlier measurements. We have examined the hysteresis properties of the balance by imposing transients with no mass change by applying electrostatic pulses with a range of amplitudes and times and examining the effect on the force after return to null. These data are summarized in Table 1. The hysteresis force is a non-linear function of excursion and time, with a large increase between 10 μm and 30 μm pulse amplitude. For our conditions, we estimate a hysteresis contribution (adding to the apparent electrostatic force) of 1.3 nN ± 0.5 nN.

All sources of uncertainty are summarized in Table 2. The raw measurement data are corrected for hysteresis and the voltmeter calibration factor and are statistically combined to yield a computed electrostatic force of 205,015.0 nN ± 4.4 nN (coverage factor, k = 1) [11]. This test mass had been previously measured by the NIST mass calibration group and assigned a value of 20.91905 mg ± 0.00035 mg (k = 1) which corresponds to a force of 205,028.3 nN ± 3.5 nN for the local gravity, measured to be 9.801033 m/s^2 ± 0.000004 m/s^2.

6. CONCLUSION

A traceable pathway for force calibrations via SI electrical units and length units has been established with an estimated uncertainty that is competitive with traditional mass-based force calibrations for a 200 μN force, and which has a force noise floor of a few nN. The difference between the measured forces is 13.3 nN, or a factor of 6.7×10^{-5}, which is greater than the k = 1 uncertainty bounds, but less than the k = 2 bounds, and should not be considered a significant discrepancy at this point.

Refinements of the EFB are underway which are expected to further reduce the noise floor and the uncertainty of force measurements by as much as a factor of ten. Spring stiffness calibrations are also continuing, and mechanisms and metrology are being added to facilitate and enhance these measurements as well. As smaller test masses are weighed, particularly as improvements are made to the EFB, the increase in the relative uncertainty of the electrostatic force measurement is expected to be less than the increase in the mass calibration relative uncertainty.

Table 2. Relative standard uncertainties in electrostatic force measurement using a 20 mg test mass.

Uncertainty sources	Contribution to total uncertainty ($\times 10^{-5}$)	
Standard transfers (type B)		
z	0.3	
V	0.6	
C	0.3	
Correction terms		Correction value ($\times 10^{-5}$)
alignments	0.05	
corner loading	0.03	
hysteresis	0.3	–0.7
Statistical (type A)		
weighing	2.0	
dC/dz	0.6	
Combined	2.2	

REFERENCES

[1] W.C. Oliver, and G.M. Pharr, "An Improved Technique for Determining Hardness and Elastic Modulus using Load and Displacement Sensing Indentation Experiments," *J. Mater. Res.*, Vol. 7, No. 6, pp. 1564–1583, 1992.

[2] J. Israelachvili, *Intermolecular and Surface Forces*, 2nd ed., Academic Press, London, 1992.

[3] M. Rief, H. Clausen-Schaumann, and H. E. Gaub, "Sequence Dependent Mechanics of Single DNA Molecules," *Nature Structural Biology*, Vol. 6, No. 4, pp. 346–349, 1999.

[4] N. A. Burnham, X. Chen, C. S. Hodges, G. A. Matei, E. J. Thoreson, C. J. Roberts, M. C. Davies, and S. J. B. Tendler, "Comparison of Calibration Methods for Atomic-Force Microscopy Cantilevers," *Nanotechnology*, Vol. 14, No. 1, pp. 1–6, 2003.

[5] J.R. Pratt, J.A. Kramar, D.B. Newell, and D.T. Smith, "Review of SI Traceable Force Metrology for Instrumented Indentation and Atomic Force Microscopy," *Meas. Sci. Technol.* Vol. 16, No. 11, pp. 2129–2137, 2005.

[6] J. A. Kramar, D. B. Newell, and J. R. Pratt, "NIST Electrostatic Force Balance Experiment,"; *Proc. of the Joint International Conference IMEKO TC3/TC5/TC20*, VDI-Berichte 1685, pp. 71–76, 2002; J.R. Pratt, D.B. Newell, and J.A. Kramar, "A Flexure Balance with Adjustable Restoring Torque for Nanonewton Force Measurement," *ibid.*, pp. 77–82.

[7] D. B. Newell, J. A. Kramar, J. R. Pratt, D. T. Smith, and E. R. Williams, “The NIST Microforce Realization and Measurement Project,” *IEEE Transactions on Instrumentation and Measurement*, Vol. 52, No. 2, pp. 508–511, 2003.

[8] J. R. Pratt, D. T. Smith, D. B. Newell, J. A. Kramar, and E. Whitenton, “Progress Toward Systeme International d'Unites Traceable Force Metrology for Nanomechanics,” *J. Mater. Res.*, Vol. 19, No. 1, pp. 366–379, 2004.

[9] P. J. Cumpson, and J. Hedley, “Accurate Analytical Measurements in the Atomic Force Microscope: A Microfabricated Spring Constant Standard Potentially Traceable to the SI,” *Nanotechnology* Vol. 14, No. 12, pp. 1279–1288, 2003.

[10] I-M. Choi, M-S. Kim, S-Y. Woo, and S-H. Kim, “Parallelism Error Analysis and Compensation for Micro-force Measurement,” *Meas. Sci. Technol.*, Vol. 15, No. 1, pp. 237–243, 2004.

[11] B. N. Taylor, and C. E. Kuyatt, “Guidelines for Evaluating and Expressing the Uncertainty of NIST Measurement Results,” *NIST Technical Note 1297*, 1994.